Check for updates

Castor oil-derived polyurethane networks multiple recyclability based on reversible dynamic acetal bond

Muhammad Abu Taher,[ab] Yi Su,[ac] Xiaolin Wang,*[a] Xiaobo Xu, [ID][ac] Md Ahsan Habib,[d] Jin Zhu*[a] and Jing Chen [ID] *[a]

Making polyurethanes (PUs) from castor oil (CO) is severely constrained because they cannot be recycled due to the irreversibly cross-linked structure. In addition, a CO-derived PU shows low strength, poor durability and inadequate utility because of its elevated cross-linking density and its soft backbone. To overcome this, using a solvent-free thiol-olefin click reaction, we initially synthesized castor oil that has been modified to become 1-thioglycerol (TCO), and then we employed this polyol to produce cross-linked polyurethanes designated TCO-NCO (NCO-HDI, HMDI, and IPDI) without adding a catalyst or solvent. They showed substantial tensile strength that was significantly greater than previously highlighted vegetable oil polyurethanes but were not recyclable. Then we developed VTCO, a combination of vanillin and TCO that occurred at an elevated temperature while the solvent and catalyst remained present. Thereafter, VTCO-NCO was employed to achieve sustainable polyurethane covalent adaptable networks (CANs) that seemed to have new reversible acetal bonds. The PUs have a high rate of stress relaxation because their structural cross-linking network is made up of dynamic acetal bonds. This research introduces a simple, ubiquitous approach that can reconcile mechanical robustness, recycling performance, chemical degradation, and an environmentally friendly way to make sustainable PUs.

1. Introduction

With regard to polyurethanes (PUs), the notably long, malleable fatty acid structure of vegetable oils makes them perfect soft segments, and the triglyceride groups and carbon–carbon double linkages provide reactive functional groups for developing and changing the structure.[1,2] The hydrophobic properties of triglyceride and the infusion of long fatty acid chains ensure that the PU films have outstanding physical and chemical properties.[3,4] There has been a great deal of progress made with regard to broadening their potential through using plant oil to develop polyurethanes that have improved hydrolysis, flexibility, and durability.[5,6] However, the recyclability of polyurethanes made from vegetable oil is being investigated by many researchers.[7,8]

Thermoset polyurethane substances have been widely utilized in a wide range of applications, such as the aviation industry,[9] tissue regeneration,[10] electronic component production,[11] and automobile industries,[12] because of their excellent mechanical characteristics,[13] high density of cross-links,[14] superb heat resistance,[15] solvent and creep stability,[16] and malleability.[17] Polyurethane's various uses have led to resource wastage and environmental damage because of the rigidity of its structures.

Covalent adaptable networks (CANs) destabilize the archetype that restricted conventional thermosetting resin, enabling it to be reused and recycled.[8,18] Dynamic covalent linkages, such as disulfide,[19,20] acetal,[21] vinylogous urethane,[22] and imine,[23] are now used in CO-derived PUs for increased flexibility, chemical degradability, and recyclability. This is accomplished by providing the covalent cross-linked network with the capacity to migrate or separate *via* dynamic covalent bond cracking or transfer.[24] Thermosetting polymers generated from vegetable-oil-based monomers typically have chemically cross-linked structures and are therefore challenging to recycle or degrade owing to their branching organization and numerous reactive sites.[25]

[a] Key Laboratory of Bio-based Polymeric Materials Technology and Application of Zhejiang Province, Laboratory of Polymers and Composites, Ningbo Institute of Materials Technology and Engineering, Chinese Academy of Sciences, Ningbo 315201, P. R. China. E-mail: wangxiaolin@nimte.ac.cn, jzhu@nimte.ac.cn, chenjing@nimte.ac.cn

[b] University of Chinese Academy of Sciences, Beijing, 100049, P. R. China

[c] School of Materials Science & Chemical Engineering, Ningbo University, Ningbo 315211, P. R. China

[d] South China Advanced Institute for Soft Matter Science and Technology, School of Emergent Soft Matter, South China University of Technology, Guangzhou 510640, China

In spite of the fact that vegetable oils are disposable and recyclable, the decomposition of their polymers in the environment is relatively slow.[26] As a result, issues related to environmental buildup and contamination from their widespread implementation have yet to be resolved.

Vanillin is a molecular phenolic compound that is synthesized in significant quantities from feedstock.[27] It has the potential to be employed in the biosynthesis of bio-based polymers, as aromatic monomers in the molecules could provide acceptable thermo-mechanical properties. Aldehyde, hydroxyl, and ether are its three functional units and there are aldehyde groups in the para position on the benzene ring.[28] By altering vanillin, it is capable of producing a great deal target product, such as polyurethane, without ever using petroleum-based raw materials, which has drawn the attention of numerous investigators.[29,30] Vanillin and lignin have been employed to create a variety of unique bio-based polyurethanes, but their poor mechanical properties and costly production methods limit their potential.[31–34]

The synthesis of a renewable epoxy with a Schiff base framework based on vanillin addition is a recognized area of research.[35] Epoxidizing compounds of vanillin bearing imine bonds and cross-linking them with some other amino group hard segment yields a reprocessable epoxy thermoset.[23,36,37] The novel epoxy resin functions comparably to a bisphenol-based epoxy resin and shows excellent biodegradation and recyclability.[38,39] A vanillin derivative of terminal diols with such a dynamic Schiff base has indeed been synthesized as a consequence of our investigations as well as to address the issues highlighted above.[40,41] Furthermore, a unique bio-based polyurethane is produced with castor oil and vanillin, so this could be a promising approach in the chemical synthesis of high-performance, biodegradable polyurethane.

A thioglycerol modified castor oil polyol (TCO) was synthesized by a solvent-free thiol-olefin click reaction employing 2-hydroxy 2,2-dimethylacetophenone as little more than a photoinitiator at low temperature in this research. Also, we are focusing on even more series of recyclable polyurethane CANs by using commonly available vanillin as a cross-linking agent for TCO-derived PU intermediates, that are constructed by simply reacting VTCO with isocyanate. The CO-derived polyurethane CANs can be utilized as environmentally friendly substitutes for renewable and recyclable polyurethanes for several purposes, including adhesives, flexible synthetic rubber, and hard polymers.

2. Method and preparation

2.1 Chemicals

Vanillin, 1-thioglycerol (≥95%), 2-hydroxy-2,2-dimethylacetophenone (1173), ethyl acetate (≥99%), sodium hydroxide (NaOH), potassium hydroxide (KOH), sodium chloride (NaCl), magnesium sulfate ($MgSO_4$), acetone, 1,1,1,3,3,3-hexafluro-2-propanol (HFP) (≥99.5%), (AR grade) were purchased from Aladdin Reagent Co., China. Castor oil (CO) (AR grade), toluene, isophorone diisocyanate (IPDI), 1,6-hexamethylene diisocyanate (HDI) (≥99%) and 4,4′-methylenedicyclohexyl diisocyanate

(HMDI) (≥90%) were purchased from Macklin Co., China. P-Toluene sulfonic acid (≥98%) was purchased from Tokyo Chemical Industries Co., Japan. Hydrochloric acid (HCl, 12 mol L^{-1}) and sodium hydroxide (NaOH) were purchased from Sinopharm Chemical Reagent Co., Ltd, China. All investigations were carried out with local water that had been deionized.

2.2 Preparation of the 1-thioglycerol modified castor oil (TCO)

Without the addition of any solvent, castor oil (CO) and 1-thioglycerol were incorporated in a 150 mL conical flask at a 1 : 3 molar ratio of double bonds to sulfhydryl groups, and 2 wt% of the photoinitiator 1173 (in comparison to the total weight of CO) was included to serve as a catalyst. Afterwards, the solution was irradiated with UV light for one hour underneath a 50 watt neon lamp in an ice cube tray. Following that, the sample was dissolved with ethyl acetate and at a minimum rinsed five times with saturated sodium chloride solution. Following the extraction of the organic layer, it was subjected to drying and filtration with magnesium sulfate. Castor-oil-derived polyol was produced after evaporating the ethyl acetate via an evaporator and ambient drying in a vacuum oven.

2.3 Preparation of vanillin modified castor oil (VTCO)

TCO (20 g) and vanillin (7.38 g) were mixed in a 150 mL conical flask with toluene as the solvent and P-toluene sulfonic acid as the catalyst. The reaction that followed was performed at 130 °C for 24 hours. To eliminate the toluene, the product was evaporated using a rotary evaporator at 70 °C. Unreacted vanillin was washed from the sample using ethyl acetate once and water twice. Next, it was rinsed with sodium bicarbonate and the ethyl acetate was taken out with a rotary evaporator machine at 55 °C for 10 minutes, and finally the VTCO was poured. Scheme 1 shows the synthesis pathway.

2.4 Preparation of polyurethane using TCO and VTCO

In the absence of both a solvent and a catalyst, TCO, VTCO, and isocyanate (IPDI, HDI, and HMDI) reacted together to produce thermosetting polyurethane compounds. The mixture of ingredients was initially thoroughly blended at 70 °C to achieve full homogeneity and transparency. The material was pre-cured on a tinplate at 80 °C for 2 hours, post-cured in a vacuum at 100 °C for 2 hours, and at 140 °C for 2 hours to produce TCO and VTCO modified castor oil PU films. The thermal and mechanical properties of the PU films were then tested. Table 1 provides a summary of the formulation of TCO and VTCO modified castor oil polyurethanes.

2.5 Characterization

2.5.1 ^{1}H NMR. Nuclear magnetic resonance (^{1}H NMR) experiments on TCO and VTCO were carried out with DMSO as the solvent throughout. A Bruker AV600 spectrometer was used in these investigations.

2.5.2 TOF-MS. The TOF-MS analysis utilized DMF as the solvent. The time-of-flight mass spectrometer was an AB Sciex Triple TOF 4600, manufactured in the United States.

Scheme 1 Synthesis route of TCO and VTCO.

Table 1 The polyurethane feed composition

Sample	Molar ratio (OH : –NCO)	Polyols (g)	HDI (g)	HMDI (g)	IPDI (g)
TCO-HDI	1:1	2	1.22		
TCO-HMDI	1:1	2		2.11	
TCO-IPDI	1:1	2			1.164
VTCO-HDI	1:1	2	0.57		
VTCO-HMDI	1:1	2		0.91	
VTCO-IPDI	1:1	2			0.64

2.5.3 Fourier transform infrared (FTIR). The FTIR spectra of the materials were captured using a Micro-FTIR Cary 660 (Agilent, United States) using the attenuated total reflection (ATR) technique.

2.5.4 Tensile test. An Instron 5567 electrical universal testing machine (Instron, USA) was employed to determine the tensile properties. The PU thermosets, TCO-NCO and VTCO-NCO, were designed with dimensions of 30 mm length, 5 mm width, and 0.4 mm thickness. This thickness was measured using a gauge length of 20 mm and a cross-head speed of 100 mm per minute. Testing of at least five samples was a guarantee of accuracy.

2.5.5 Dynamic mechanical analysis (DMA). The storage modulus and tan δ of the polyurethane (PU) films were evaluated through dynamic mechanical analysis (DMA) according to

tensile conditions with a Q800 DMA dynamic mechanical analyzer (TA Instruments). The samples should measure 20 mm in length, 5 mm in width, and 0.4 mm in thickness for the purpose of analysis. After cooling with liquid nitrogen, the samples were kept at the −60 °C isotherm for three minutes. After that, the samples were heated to 180 °C at a rate of 5 °C min^{-1} with a frequency of 1 Hz. The cross-linking densities of the polyurethanes (ρ) were determined using eqn (1).[42,43]

$$\rho = \frac{E'}{3RT} \tag{1}$$

where T is the Kelvin temperature at T_g + 30 °C, R is the gas constant, and E' is the polyurethane storage modulus at T_g + 30 °C.

2.5.6 Differential scanning calorimetry (DSC). To figure out the T_g values, an MET DSC from Mettler Toledo in Switzerland was utilized. The sample was initially heated from room temperature to 180 °C and maintained there for ten minutes in order to remove its thermal history. The temperature was raised to 180 °C to generate a second heating curve (heating rate of 20 °C min^{-1}), whose differential curve displays a peak identical to T_g after cooling to room temperature at a rate of 50 °C min^{-1}.

2.5.7 Thermogravimetric analysis (TGA). A TGA/DSC1 thermogravimetric analyzer (Mettler Toledo, Switzerland) was used to determine the thermal stability of the samples. With nitrogen as the gas environment, the scanner temperature was increased by 20 °C per minute from 50 to 800 °C.

2.5.8 Stress relaxation test. A DMAQ850 instrument, manufactured by TA (USA), was used to test the VTCO-IPDI samples. During testing, the tensile frequency was 1 Hz. Initially, a preload of 0.001 N was applied during the heating process. Once the test temperature had been attained, the temperature was held constant for 2 minutes to achieve thermal equilibrium. After that, we put the sample through some stress. The strain in the reference sample was always kept at 2.5%. During the measurement, the time-dependent change in the relaxation modulus was recorded.

2.5.9 Degradation of VTCO-NCO. A 30 mm × 5 mm × 0.6 mm sample of VTCO-IPDI was submerged in both acid and base in an acetone and HFP solution. The weight of the specimen before and after its degradation were measured after drying in a vacuum chamber at 70 °C for an appropriate duration, and were utilized to determine the rate of degradation.

3. Results and discussion

3.1 ^{1}H NMR, FTIR and TOF-MS of TCO and VTCO

Castor-oil-based TCO and VTCO were characterized using ^{1}H NMR, TOF-MS, and FTIR to determine the associated molecular structures. The ^{1}H NMR spectra of TCO peaks at 4.36 ppm and 4.11 ppm shown in Fig. 1a correspond to those of VTCO phenolic OH peaks at 9.11 ppm, as shown in Fig. 1b. The ^{1}H NMR of the benzene ring on the molecular framework of vanillin is represented by the peaks at 6.75 and 7.07 ppm, as shown in Fig. 1b. The thioether products (–CH$_2$–S– and –CH–S–) have peaks at 2.36–2.45 ppm and 2.53–2.84 ppm, as shown in Fig. 1a and b. The ^{1}H NMR signal from the methyl group in the
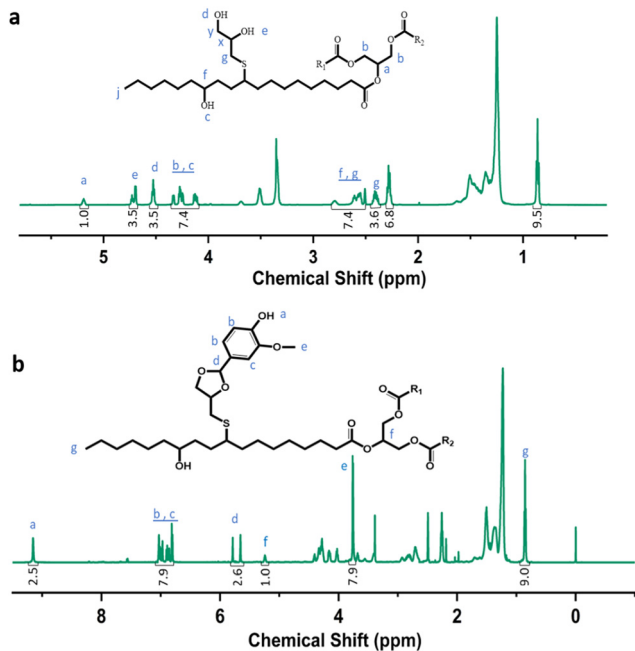
Fig. 1 Characterization of the structure of TCO and VTCO. (a) ^{1}H NMR spectrum of TCO. (b) ^{1}H NMR spectrum of VTCO.

vanillin structure appears as a peak at 3.76 ppm, whereas the peaks from the acetal structure appear at 5.79 and 5.65 ppm, as shown in Fig. 1b. The characteristic peaks of the OH structure of VTCO become lower than those of TCO in the FTIR spectra, as shown in Fig. 2a. The stretching vibration of the C–O–C acetal bond in the VTCO spectrum can be observed at 1116 cm^{-1} in Fig. 2a, confirming the presence of an acetal structure. The results of mass spectrometry (TOF-MS) in Fig. 2b and c show that the molecular weight (MW) of VTCO, a castor-oil-based polyol containing an acetal structure, has risen considerably, and is approximately equal to the theoretical molecular weight of the compound. This further indicates the successful synthesis of castor oil polyol VTCO containing an acetal structure.

3.2 Dynamic mechanical analysis (DMA) and differential scanning calorimetry (DSC)

DMA is a useful platform for investigating how the structure of the hard and soft segments, as well as their interaction, affect the physical and mechanical properties of the polymer chain network. Temperature-induced changes in the cross-linking density (ρ), storage modulus, and loss tangent ($\tan \delta$) are depicted in Fig. 3a and b. The decreased storage modulus of VTCO-NCO compared to that of TCO-NCO may be caused by the incorporation of vanillin into the polymer chains, which facilitated the mobility of the molecular chains and caused the hard segment to become less restricted.

The storage modulus for VTCO-IPDI was 1664 MPa at a temperature of 30 °C due to the unique interactions between the surface hydroxy group of VTCO and the isocyanate (Table 2). TCO-NCO led to a higher T_g than VTCO-NCO because acetal bonding decreases the backbone rigidity. A more flexible vanillin-based heterocyclic acetal structure could also contribute to the reduced

T_g.[44,45] The cross-linked density of TCO-NCO is considerably greater than that of VTCO-NCO. The reduction in cross-linking density restricted the chain segment movement of the polymeric material, and that effect was compounded by a boost in the amount of stiff TCO-NCO among the polymeric chain segments of the polyurethane, which additionally increased chain segment movement.[43] Overall, chain segment mobility was constricted in TCO-NCO compared to that in VTCO-NCO. By including the bifunctional structure of vanillin, the cross-linking density of VTCO-NCO dropped.[46–48] The glass transition temperature (T_g) of the thermosetting polyurethanes measured by DSC is shown in Fig. 3c and d. In Fig. 3c and d it can be seen that the T_g of samples TCO-HDI, TCO-HMDI and TCO-IPDI are 49.4 °C, 65.8 °C and 72.4 °C, and castor-oil-based thermosetting polyurethane resins on an acetal structure showed a significant upward trend: 22.6 °C, 28.4 °C and 37.4 °C for VTCO-HDI, VTCO-HMDI and VTCO-IPDI, respectively.

3.3 Thermogravimetric analysis (TGA)

The thermal stability of the bio-based polyurethane was measured by TGA. The results are shown in Fig. 4 and the samples show excellent thermal stability. The vanillin linked with a CAN base can address the thermal stability, as demonstrated by the starting decomposition temperature 5% weight loss of VTCO-HDI, VTCO-HMDI and VTCO-IPDI of 208.2 °C, 212.3 °C and 219.3 °C, as shown in Fig. 4. Consequently, the initial degradation of the VTCO-NCO phase at about 170 °C is due to the breakage of the urethane bond, whereas the next degradation phase at around 280 °C is due to the breaking of the ester bond components in castor oil. The 5% weight loss temperatures for TCO-HDI, TCO-HMDI and TCO-IPDI are 281.7 °C, 283.3 °C and 285.6 °C. According to the materials taking part in the study, the six-membered heterocyclic structure of VTCO may have the ability to minimize the early thermal degradation rate of the plastic.[49,50]

3.4 Strain–stress relaxation

Different temperatures were employed in the stress–relaxation tests. Even with the reference TCO-NCO which is devoid of aromatic vanillin, its network cannot be changed. The fundamental cause of the stress relaxation that the cross-linked polyurethane exhibits is that the reaction takes place through the mechanism of dynamic covalent bonding throughout the cross-linked network. To further investigate the dynamical repeatability of the C–O–C acetal bond in the VTCO-IPDA cross-linked matrix, various stress–relaxation properties of VTCO-IPDA have been addressed in Fig. 5. According to the Maxwell model, the stress–relaxation time (τ^*) is defined as the amount of time following which $1/e$ (i.e., 0.37) has completely replaced the original modulus. When the temperature rises, the stress relaxation of VTCO-IPDA accelerates. For instance, at 190, 200, and 210 °C, τ^* reduced to 12 238, 5702, and 3938 s, respectively, as shown in Fig. 5b. The curve of stress–relaxation time τ^* with $1000/T$ at different temperatures is shown in Fig. 5a. The relaxation process follows the Arrhenius eqn (2).[51,52]

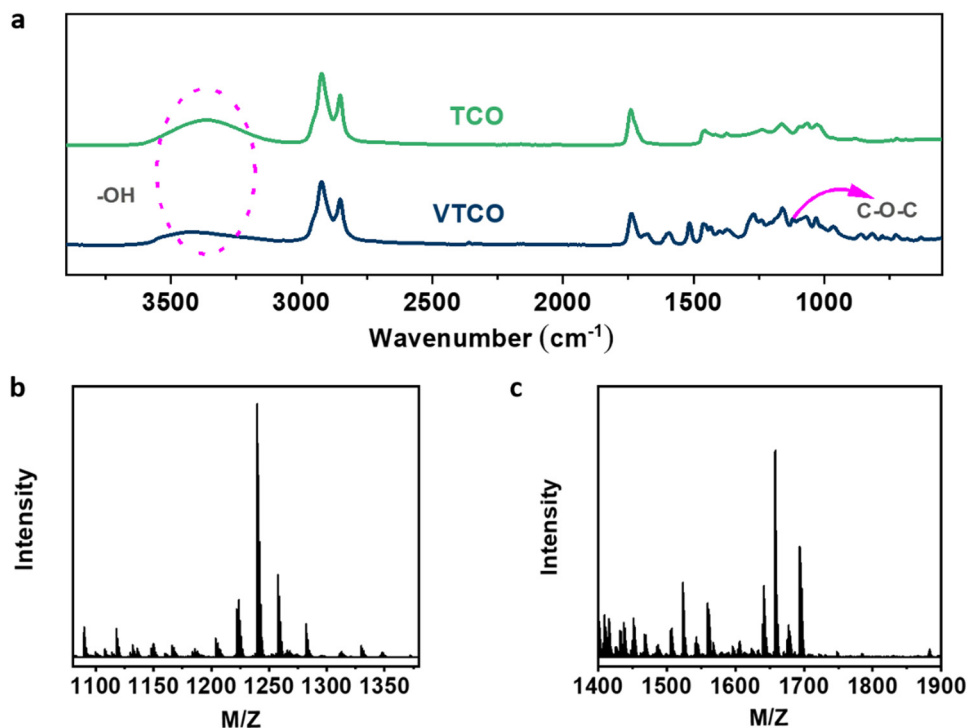$$\tau^*(T) = \tau_0 \exp\left(\frac{E_a}{RT}\right) \tag{2}$$

Fig. 2 (a) FTIR spectra of TCO and VTCO. (b) TOF-MS spectrum of TCO. (c) TOF-MS spectrum of VTCO.

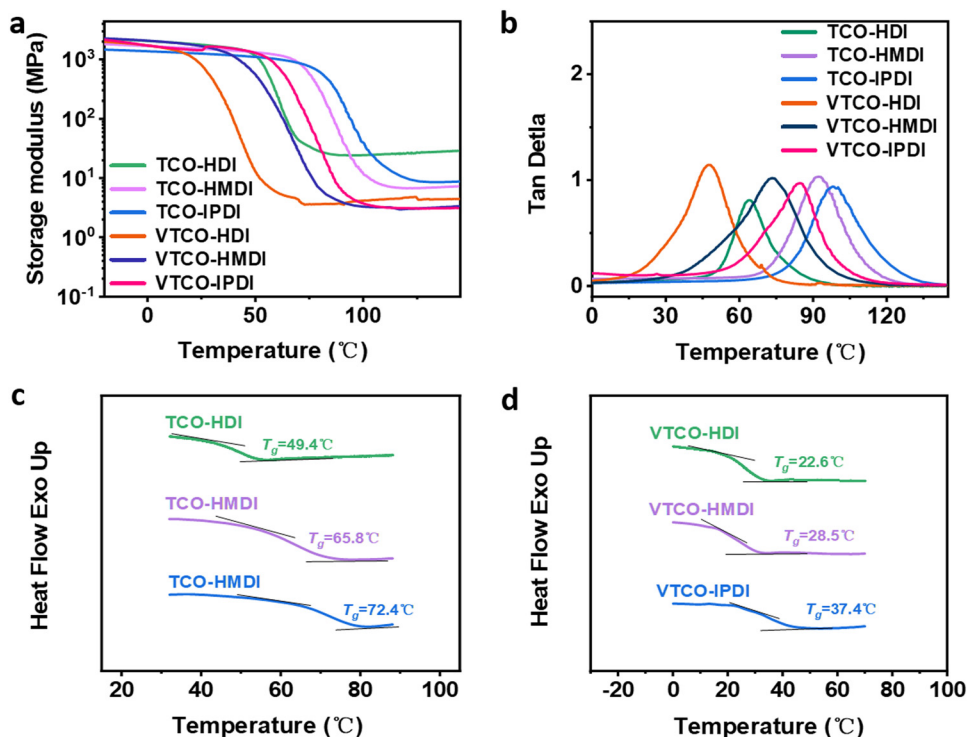**Fig. 3** (a) Storage modulus and (b) tan δ as a function of temperature for TCO-NCO and VTCO-NCO by DMA. (c) DSC curve of TCO-NCO. (d) DSC curve of VTCO-NCO.

where τ_0 is the pre-exponential factor of the Arrhenius equation, R is the ideal gas constant (R = 8.314 J K^{-1} mol^{-1}), T is the test temperature (Kelvin temperature), and E_a is the exchange reaction energy in the network. According to the relaxation time test

Table 2 Thermal properties of castor-oil-based polyurethane

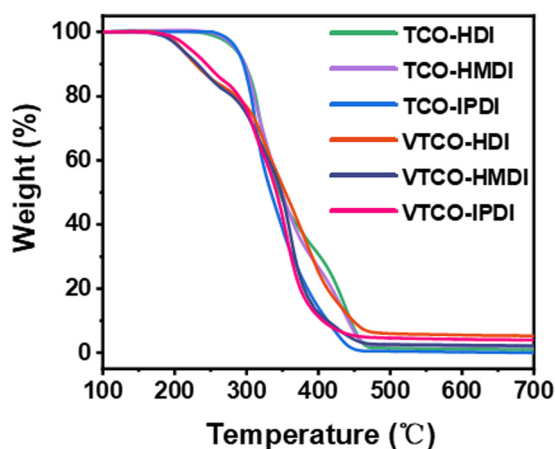| Sample	Storage modulus at 30 °C (MPa)	T_g (°C) DMA	DSC	ρ (mol m^{-3})
TCO-HDI	1690	63.56	49.4	635.16
TCO-HMDI	1482	92.12	65.8	681.94
TCO-IPDI	1225	98.52	72.4	849.58
VTCO-HDI	462	46.76	22.6	412.58
VTCO-HMDI	1538	73.23	28.4	342.37
VTCO-IPDI	1664	83.63	37.4	324.16

Fig. 4 TGA curves of TCO-NCO and VTCO-NCO.

results, the exchange activation energy E_a of the reconfigurable castor-oil-based thermosetting polyurethane resin VTCO-IPDI based on an acetal structure is 100.54 kJ mol^{-1} by fitting the slope of the Arrhenius equation.

The quick exchange of dynamic covalent bonds that occurs as the temperature rises, which induces the reconfiguration of a cross-linked network architecture, seems to be the cause of the increase in stress–relaxation rates. The activation energy is greater than the value for polyurethane containing constrained covalent bonds, but is comparable to that of poly(urethane–urea) containing alternative dynamic covalent bonds.[53] These

findings back up the hypothesis that the dynamic interchange in covalent bonds is responsible for the stress–relaxation activity of VTCO-IPDI. The recyclability of VTCO-IPDA based on covalent bonds is benefited by this exchange reaction.

3.5 Tensile strength

Due to the variable backbone rigidity and cross-linking density, TCO-NCO and VTCO-NCO are predicted to have adjustable dynamic mechanical characteristics. Our TCO-NCO specimen demonstrated a good tensile modulus and, according to Fig. 6a and b and films, the mechanical properties of TCO-NCO were drastically improved. The tensile properties of VTCO-HDI, VTCO-HMDI, and VTCO-IPDI are 17.41, 40.80, and 46.44 MPa, which are significantly less than the values for TCO-HDI, TCO-HMDI, and TCO-IPDI, which are 51.5, 62.2, and 83.87 MPa, as shown in Table 3. The mechanical characteristics of the PU film are significantly reduced because of the incorporation of vanillin in VTCO. These characteristics resemble those of bio-based polyurethane, which is biodegradable, strong, and reprocessable.[23,54] The tensile behavior of VTCO-NCO combinations ranged from the capabilities of a flexible elastomer to those of a robust and even hard composite material. By amending the formula, we are able to produce TCO-NCO and VTCO-NCO with mechanical properties that transform the features of an elastomer into those of a strong and hard plastic, respectively. These materials have the potential to be used in a variety of applications. Because of this, biodegradable plastics synthesized from CO have a broad spectrum of applications.

3.6 Fourier transform infrared (FTIR)

FTIR was employed to figure out the structures of TCO, VTCO, TCO-NCO, and VTCO-NCO, and the results are shown in Fig. 7a and b. The strong peak of –OH at 3400 cm^{-1} for TCO and VTCO disappeared from the spectra of TCO-NCO and VTCO-NCO. The peaks for TCO-NCO at 3336 cm^{-1} and VTCO-NCO at 3347 cm^{-1}, which have been attributed to the N–H stretching vibrations, indicate the effective fabrication of a urethane unit. The FTIR spectrum may be employed to evaluate the hydrogen bond
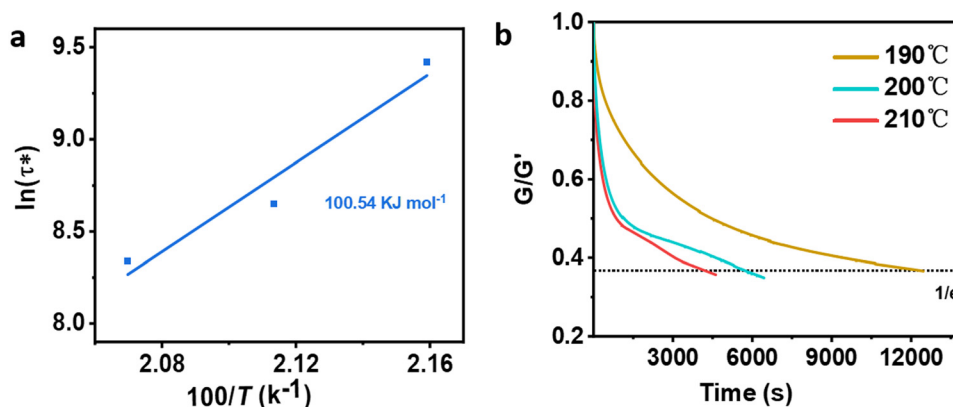

Fig. 5 (a) Fitted Arrhenius equation of VTCO-IPDA according to the experimental data. (b) Stress–relaxation curves of VTCO-IPDA at different temperatures after normalization.
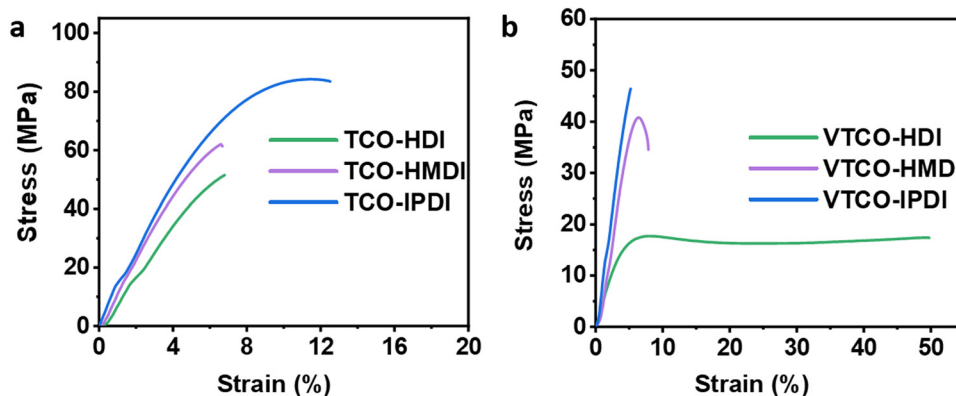
Fig. 6 Representative stress−strain curves of (a) TCO-NCO and (b) VTCO-NCO.

Table 3 Mechanical characteristics of castor oil-based polyurethanes

Sample	Tensile modulus (MPa)	Tensile strength (MPa)	Elongation at break (%)
TCO-HDI	1004.4	51.5	6.8
TCO-HMDI	1266.4	62.2	6.7
TCO-IPDI	1449.7	83.87	12.6
VTCO-HDI	257.02	17.4	49.7
VTCO-HMDI	149.89	40.8	7.8
VTCO-IPDI	192.74	46.4	5.2

strength. Typically, a smaller wavenumber for the $C{=}O$ stretching vibration denotes stronger hydrogen bonding.[55,56] The new $C{=}O$ stretching peak, with significant absorption of TCO-NCO and VTCO-NCO within 1690 cm^{-1} and 1700 cm^{-1}, suggests the development of urethane. The stretching vibration of C–O–C in the acetal bond can be recognized in the spectra of both VTCO and VTCO-NCO, demonstrating the presence of an acetal structure in VTCO-NCO. The results showed that the reaction between TCO and VTCO with the NCO group was successful in producing polyurethane.

3.7 Recyclability of VTCO-IPDA

A conventional thermoset may be easily recycled if the materials include dynamic bonds that can be reconstructed in

reaction to a specific trigger (Scheme 2). The inclusion of acetal bonds permits thermoset polymers to undergo post-processing and recycling in a short amount of time at elevated temperature. VTCO-IPDA can also go through multiple processing cycles and maintain its existing material properties as much as possible, as shown in Fig. 8a. This is because its affiliation method is based on network reshuffling rather than network disconnection. Further evidence showed that VTCO-IPDA maintained the stability of its engineering properties derived from the almost absolute lack of change in the FTIR spectra curve following two processing cycles, as well as the characteristic peak of the acetal bond continuing to be present continuously at 1120 cm^{-1} in Fig. 8b. The mechanical characteristics of the material remained high even after two hot-pressing cycles.

As shown in Fig. 8c and Table 4, the highest tensile modulus, tensile strength, and elongation at break all decreased by 31.83%, 12.57%, and 21.15%, respectively, of their original values after the 1st recycle.

3.8 Degradation of VTCO-IPDI

The material may degrade when it is no longer necessary to sustain performance during actual use. Polyurethane degradation has long been a problematic issue. Polyurethane waste is processed by dumping or burial, which contaminates the environment and destroys the soil. Traditional polyurethane
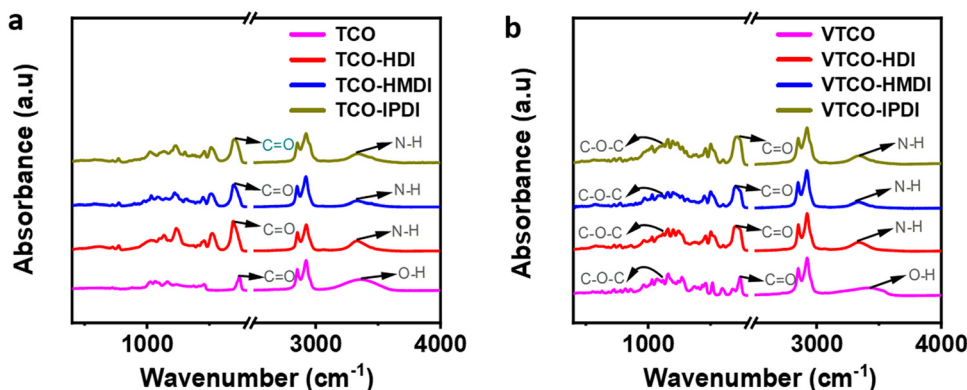

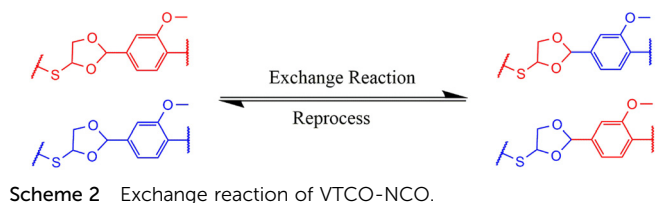Fig. 7 FTIR spectra of (a) TCO-NCO and (b) VTCO-NCO.

Scheme 2 Exchange reaction of VTCO-NCO.

degrades chemically in a severe manner. On the other hand, VTCO-NCO which does contain the CAN group has a propensity for specific features associated with degradation. VTCO-IPDI, which is depicted in Fig. 10, has cyclic acetal groups that make it degradable. VTCO-IPDI, of dimensions of 30 mm × 5 mm × 0.6 mm, was tested for gradual degradation in a solution of 1 M HCl H_2O/HFP (1/9, v/v) at a temperature of 60 °C for zero minutes to two hours, as shown in Fig. 9. The volume of VTCO-IPDI was shown to have boomed initially, reduced with time, and eventually entirely degraded. The breakdown of the solid causes the solution to turn from colorless to reddish-yellow. We hypothesize that VTCO-IPDI degradation was initially dominated by swelling, followed by breakdown of the cross-linked network and dissolution of the swelling surface into the solution. As a result, the expansion and rates of decomposition of the cross-linked matrix have to be assessed continuously to manage the degradation rate. An acetone experiment, where the volume ratio of water to organic solvent was 1 : 9, confirmed that the sample did not degrade in the acetone system. While 1 M NaOH H_2O/acetone solution (1/9, v/v) solution employed at 60 °C for 5 h degraded the cross-linked structure and dispersed

Table 4 The reprocessing of the mechanical characteristics of castor-oil-based polyurethanes

Sample	Tensile modulus (MPa)	Tensile strength (MPa)	Elongation at break (%)
VTCO-IPDI	192.74	46.44	5.2
V-TCO-IPDI-Re-1	119.75	40.60	4.1
V-TCO-IPDI-Re-2	233.84	36.66	3.3

Fig. 9 Degradation process of VTCO-IPDI at different times in a 1 M HCl H_2O/HFP (1/9, v/v) solution.

the expanding surfaces into the solution, but there was no degradation when the experiment used HFP. Furthermore, the incorporation of acetal connections renders it feasible for the material to degrade chemically rapidly in moderate conditions.
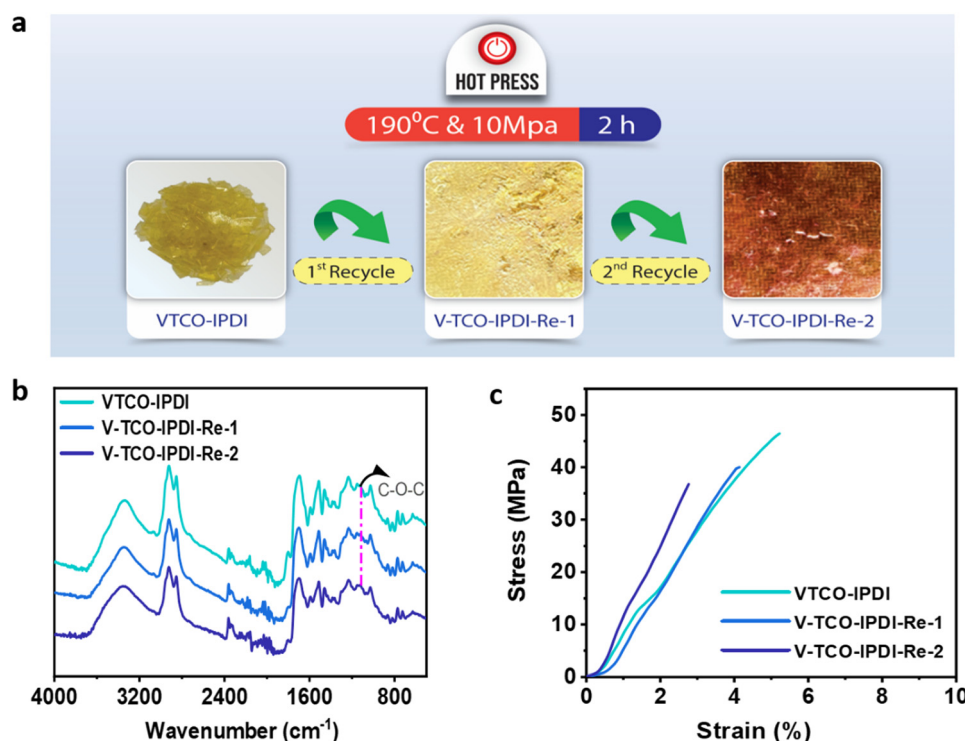

Fig. 8 (a) Recycling by hot pressing. (b) FTIR spectra of reprocessed VTCO-IPDA. (c) Stress–strain curves of reprocessed VTCO-IPDA.

© 2024 The Author(s). Published by the Royal Society of Chemistry

Fig. 10 (a) Degradation rate of VTCO-IPDI in 1 M HCl or 1 M NaOH solutions (H$_2$O/solvent = 1/9, v/v). (b) Degradation time in 1 M HCl or 1 M NaOH solutions (H$_2$O/solvent = 1/9, v/v) at 60 °C.

4. Conclusions

The PUs exhibit outstanding mechanical properties, relaxation times, thermal processability and chemical degradation according to the acetal bond exchange interaction. Following several cycles of breaking and thermal reprocessing, the network architecture and mechanical characteristics remained essentially unmodified. The products may also endure through two recycling steps and still retain up to 79% of their initial breaking strength. This research might provide a framework for the development and production of innovative polymeric matrices derived from different vegetable oils that really are sustainable, recyclable and also chemically degradable.

Author contributions

Muhammad Abu Taher: investigation, data curation, writing original draft, visualization. Yi Su: conceptualization, validation. Xiaolin Wang: review & editing. Xiaobo Xu: investigation, data curation. Md Ahsan Habib: data curation, draft review. Jin Zhu: funding acquisition, supervision. Jing Chen: project administration, review & editing.

Conflicts of interest

The authors declare no conflict of interest.

Acknowledgements

References

1 Y. Xia and R. C. Larock, *Green Chem.*, 2010, **12**, 1893–1909.
2 L. Maisonneuve, T. Lebarbé, E. Grau and H. Cramail, *Polym. Chem.*, 2013, **4**, 5472–5517.
3 P. M. Paraskar, M. S. Prabhudesai, V. M. Hatkar and R. D. Kulkarni, *Prog. Org. Coat.*, 2021, **156**, 106267.
4 T. Gurunathan and R. Arukula, *Polym. Degrad. Stab.*, 2018, **150**, 122–132.
5 M. A. Sawpan, *J. Polym. Res.*, 2018, **25**, 184.
6 D. P. Pfister, Y. Xia and R. C. Larock, *ChemSusChem*, 2011, **4**, 703–717.
7 D.-M. Xie, X.-L. Zhao, Y.-D. Li, Y. Weng and J.-B. Zeng, *Ind. Crops Prod.*, 2022, **188**, 115739.
8 X.-Z. Wang, D.-M. Xie, X.-L. Zhao, Y.-D. Li and J.-B. Zeng, *Macromolecules*, 2022, **55**, 2243–2251.
9 S. Wang, Z. Liu, L. Zhang, Y. Guo, J. Song, J. Lou, Q. Guan, C. He and Z. You, *Mater. Chem. Front.*, 2019, **3**, 1833–1839.
10 L. P. Gabriel, M. E. M. Dos Santos, A. L. Jardini, G. N. Bastos, C. G. Dias, T. J. Webster and R. Maciel Filho, *Nanomedicine*, 2017, **13**, 201–208.
11 J. Zhang, C. Zhang and S. A. Madbouly, *J. Appl. Polym. Sci.*, 2015, **132**, 41751.
12 S. M. Husainie, S. U. Khattak, J. Robinson and H. E. Naguib, *Ind. Eng. Chem. Res.*, 2020, **59**, 21745–21755.
13 L. Liu, J. Lu, Y. Zhang, H. Liang, D. Liang, J. Jiang, Q. Lu, R. L. Quirino and C. Zhang, *Green Chem.*, 2019, **21**, 526–537.
14 Z. Geng, A. Pang, T. Ding, X. Guo, R. Yang, Y. Luo and J. Zhai, *Macromolecules*, 2022, **55**, 8749–8756.
15 H. Xu, J. Tu, G. Xiang, Y. Zhang and X. Guo, *Macromol. Chem. Phys.*, 2020, **221**, 2000273.
16 J. Han, Y. Zhou, G. Bai, W. Wei, X. Liu and X. Li, *Mater. Chem. Front.*, 2022, **6**, 503–511.
17 X.-Z. Wang, M.-S. Lu, J.-B. Zeng, Y. Weng and Y.-D. Li, *Green Chem.*, 2021, **23**, 307–313.
18 Q. Li, S. Ma, P. Li, B. Wang, H. Feng, N. Lu, S. Wang, Y. Liu, X. Xu and J. Zhu, *Macromolecules*, 2021, **54**, 1742–1753.

19 W. Kong, Y. Yang, Y. Wang, H. Cheng, P. Yan, L. Huang, J. Ning, F. Zeng, X. Cai and M. Wang, *J. Mater. Chem. A*, 2022, **10**, 2012–2020.

20 J.-H. Chen, D.-D. Hu, Y.-D. Li, F. Meng, J. Zhu and J.-B. Zeng, *Polymer*, 2018, **143**, 79–86.

21 Y. Zhang, L. Zhang, G. Yang, Y. Yao, X. Wei, T. Pan, J. Wu, M. Tian and P. Yin, *J. Mater. Sci. Technol.*, 2021, **92**, 75–87.

22 W. Denissen, G. Rivero, R. Nicolaÿ, L. Leibler, J. M. Winne and F. E. Du Prez, *Adv. Funct. Mater.*, 2015, **25**, 2451–2457.

23 Y. Sun, D. Sheng, H. Wu, X. Tian, H. Xie, B. Shi, X. Liu and Y. Yang, *Polymer*, 2021, **233**, 124208.

24 Y. Cai, H. Zou, S. Zhou, Y. Chen and M. Liang, *ACS Appl. Polym. Mater.*, 2020, **2**, 3977–3987.

25 X. Liu, Y. Li, X. Fang, Z. Zhang, S. Li and J. Sun, *ACS Mater. Lett.*, 2022, **4**, 554–571.

26 J. N. Hahladakis, C. A. Velis, R. Weber, E. Iacovidou and P. Purnell, *J. Hazard. Mater.*, 2018, **344**, 179–199.

27 B. G. Harvey, A. J. Guenthner, H. A. Meylemans, S. R. Haines, K. R. Lamison, T. J. Groshens, L. R. Cambrea, M. C. Davis and W. W. Lai, *Green Chem.*, 2015, **17**, 1249–1258.

28 M. Wang, C. Liu, X. Xu and Q. Li, *Chem. Phys. Lett.*, 2016, **654**, 41–45.

29 B. M. Upton and A. M. Kasko, *Chem. Rev.*, 2016, **116**, 2275–2306.

30 Y. Shen, N. Xu, Y. A. Adraro, B. Wang, Y. Liu, W. Yuan, X. Xu, Y. Huang and Z. Hu, *ACS Sustainable Chem. Eng.*, 2020, **8**, 1943–1953.

31 J. A. Pinto, I. P. Fernandes, V. D. Pinto, E. Gomes, C. F. Oliveira, P. C. Pinto, L. M. Mesquita, P. A. Piloto, A. E. Rodrigues and M.-F. Barreiro, *Energies*, 2021, **14**, 3825.

32 X. Ma, J. Chen, J. Zhu and N. Yan, *Macromol. Rapid Commun.*, 2021, **42**, 2000492.

33 M. Fache, B. Boutevin and S. Caillol, *Green Chem.*, 2016, **18**, 712–725.

34 Z. Wang, P. Gnanasekar, S. Sudhakaran Nair, R. Farnood, S. Yi and N. Yan, *ACS Sustainable Chem. Eng.*, 2020, **8**, 11215–11223.

35 D.-M. Xie, D.-X. Lu, X.-L. Zhao, Y.-D. Li and J.-B. Zeng, *Ind. Crops Prod.*, 2021, **174**, 114198.

36 S. Zhao and M. M. Abu-Omar, *Macromolecules*, 2018, **51**, 9816–9824.

37 W. Yang, H. Ding, W. Zhou, T. Liu, P. Xu, D. Puglia, J. M. Kenny and P. Ma, *Compos. Sci. Technol.*, 2022, **230**, 109776.

38 N. Karak, *Sustainable epoxy thermosets and nanocomposites*, ACS Publications, 2021, pp. 1–36.

39 B. Wang, S. Ma, X. Xu, Q. Li, T. Yu, S. Wang, S. Yan, Y. Liu and J. Zhu, *ACS Sustainable Chem. Eng.*, 2020, **8**, 11162–11170.

40 K. Sykam, S. Sivanandan and P. Basak, *Prog. Org. Coat.*, 2023, **178**, 107475.

41 F. M. Haque, J. S. Ishibashi, C. A. Lidston, H. Shao, F. S. Bates, A. B. Chang, G. W. Coates, C. J. Cramer, P. J. Dauenhauer and W. R. Dichtel, *Chem. Rev.*, 2022, **122**, 6322–6373.

42 J. Dai, S. Ma, Y. Wu, L. Han, L. Zhang, J. Zhu and X. Liu, *Green Chem.*, 2015, **17**, 2383–2392.

43 X. Xu, S. Ma, J. Wu, J. Yang, B. Wang, S. Wang, Q. Li, J. Feng, S. You and J. Zhu, *J. Mater. Chem. A*, 2019, **7**, 15420–15431.

44 S. Rajendran, R. Raghunathan, I. Hevus, R. Krishnan, A. Ugrinov, M. P. Sibi, D. C. Webster and J. Sivaguru, *Angew. Chem.*, 2015, **127**, 1175–1179.

45 S. K. Yadav, K. M. Schmalbach, E. Kinaci, J. F. Stanzione III and G. R. Palmese, *Eur. Polym. J.*, 2018, **98**, 199–215.

46 S. Wang, S. Ma, C. Xu, Y. Liu, J. Dai, Z. Wang, X. Liu, J. Chen, X. Shen and J. Wei, *Macromolecules*, 2017, **50**, 1892–1901.

47 S. Engelen, A. A. Wróblewska, K. De Bruycker, R. Aksakal, V. Ladmiral, S. Caillol and F. E. Du Prez, *Polym. Chem.*, 2022, **13**, 2665–2673.

48 A. R. de Luzuriaga, J. M. Matxain, F. Ruipérez, R. Martin, J. M. Asua, G. Cabañero and I. Odriozola, *J. Mater. Chem. C*, 2016, **4**, 6220–6223.

49 B. Wang, S. Ma, Q. Li, H. Zhang, J. Liu, R. Wang, Z. Chen, X. Xu, S. Wang and N. Lu, *Green Chem.*, 2020, **22**, 1275–1290.

50 K. Tachibana and H. Abe, *Polym. Degrad. Stab.*, 2019, **167**, 283–291.

51 H. Feng, S. Ma, X. Xu, Q. Li, B. Wang, N. Lu, P. Li, S. Wang, Z. Yu and J. Zhu, *Green Chem.*, 2021, **23**, 9061–9070.

52 Y. Liu, Z. Yu, X. Xu, B. Wang, H. Feng, P. Li, J. Zhu and S. Ma, *Macromol. Rapid Commun.*, 2022, **43**, 2200379.

53 S. Wang, Y. Yang, H. Ying, X. Jing, B. Wang, Y. Zhang and J. Cheng, *ACS Appl. Mater. Interfaces*, 2020, **12**, 35403–35414.

54 Q. Li, S. Ma, S. Wang, Y. Liu, M. A. Taher, B. Wang, K. Huang, X. Xu, Y. Han and J. Zhu, *Macromolecules*, 2020, **53**, 1474–1485.

55 X. Zhou, C. Fang, W. Lei, J. Du, T. Huang, Y. Li and Y. Cheng, *Sci. Rep.*, 2016, **6**, 1–13.

56 C. Zhang, H. Liang, D. Liang, Z. Lin, Q. Chen, P. Feng and Q. Wang, *Angew. Chem., Int. Ed.*, 2021, **60**, 4289–4299.